

# Reversal of tracer advection and Hall drift in an interacting chiral fluid

Erik Kalz,<sup>1,\*</sup> Shashank Ravichandir,<sup>2,3,\*</sup> Johannes Birkenmeier,<sup>1</sup> Ralf Metzler,<sup>1,4,†</sup> and Abhinav Sharma<sup>2,5,‡</sup>

<sup>1</sup>University of Potsdam, Institute of Physics and Astronomy, D-14476 Potsdam, Germany

<sup>2</sup>Leibniz-Institute for Polymer Research, Institute Theory of Polymers, D-01069 Dresden, Germany

<sup>3</sup>Technical University of Dresden, Institute for Theoretical Physics, D-01069 Dresden, Germany

<sup>4</sup>Asia Pacific Centre for Theoretical Physics, KR-37673 Pohang, Republic of Korea

<sup>5</sup>University of Augsburg, Institute of Physics, D-86159 Augsburg, Germany

Chiral fluids are defined by broken mirror or time-reversal symmetry, giving rise to tensorial transport coefficients with antisymmetric components. A key example is the odd mobility tensor, which governs the response of a chiral tracer to an applied force and induces a characteristic transverse drift. While this response is well understood in the infinite dilution limit, the impact of interparticle interactions on the tracer dynamics remains largely unexplored. Here, we conduct an analytical and computational study of a chiral fluid with interparticle interactions and show that, under an external driving force, a chiral tracer can undergo a complete reversal of both its transverse Hall drift and its advection along the force. This reversal emerges from the interplay between odd mobility and interaction-mediated forces, resulting in a phenomenon reminiscent of absolute negative mobility.

*Introduction.* Chiral fluids have garnered significant attention for their unconventional transport properties, with no counterparts in conventional fluids. These systems exhibit striking effects, such as edge flows and optimal transport occurring at boundaries [1–4] and interactions—even purely repulsive ones—enhancing rather than suppressing motion [5–8]. The origin of these anomalous behaviors lies in the broken mirror or time-reversal symmetry inherent to chiral fluids. These unusual transport properties manifest themselves across a diverse range of systems, from condensed matter settings like magnetic skyrmion structures [9–12] and externally driven colloidal or macroscopic assemblies [13–17] to biological systems featuring self-propelled chiral agents such as *Escherichia coli* [18–20], *Thiovulum majus* [21], *Paenibacillus vortex* [22], or swimming starfish embryos [23]. Further examples include vortex fluids [24, 25] and even granular systems such as strongly rotating or magnetized plasmas [26, 27].

A unifying framework has recently emerged to describe the transport properties of these diverse chiral systems using so-called *odd* transport tensors. At the continuum level, chiral fluids are effectively characterized by concepts such as odd viscosity [28–32], while on the discrete agent-based scale, their dynamics are described in terms of odd mobility [33, 34] and odd diffusion [5, 35, 36]. The defining feature of odd transport coefficients is their tensorial structure, which includes antisymmetric off-diagonal elements that directly arise from the fundamental symmetry principles of two-dimensional rotation [37] and encode the chiral nature of the fluid. Specifically, the odd mobility tensor is given by [34]

$$\boldsymbol{\mu} = \mu_0(\mathbf{1} + \kappa\boldsymbol{\epsilon}), \quad (1)$$

where  $\mathbf{1}$  denotes the identity tensor and  $\boldsymbol{\epsilon}$  represents the totally antisymmetric Levi-Civita symbol in two dimensions. The mobility tensor relates the response velocity  $\mathbf{v}$  of a tracer to an applied force  $\mathbf{f}$  through  $\mathbf{v} = \boldsymbol{\mu}\mathbf{f}$ .

In Eq. (1)  $\mu_0$  is the bare mobility with dimensions  $[\mu_0] = \text{s/kg}$  and  $\kappa$  is the dimensionless characteristic *odd-mobility* coefficient.

In the absence of interactions, the response of a chiral tracer to an applied force follows directly from the odd mobility tensor. For a drift force  $\mathbf{f} = f\hat{\mathbf{e}}_x$ , the tracer moves with velocity  $\mathbf{v} = \mu_0 f(1, -\kappa)^\text{T}$ , exhibiting a characteristic component transverse to the driving force. This motion, commonly associated with effects such as Hall viscosity [39–41], the skyrmion Hall effect [42, 43], or lift forces in chiral flows [44, 45], is an intrinsic feature of odd mobility. While this behavior is well understood in the infinite dilution limit, the impact of interparticle interactions on the tracer’s drift in a chiral fluid remains an open problem. In this work, we systematically investigate this problem using analytical theory and simulations. By incorporating interactions within a chiral fluid, we reveal that a driven tracer can undergo a complete reversal of both its intrinsic Hall drift and its advection along the direction of the force—a striking effect reminiscent of absolute negative mobility [46, 47]. In particular, we show that these effects emerge due to the interplay of interparticle interactions and their odd mobility, which govern how the driving force is mediated through the fluid. Importantly, our theoretical framework respects the fluctuation-dissipation relation (FDR), implying that these unconventional transport phenomena arise within equilibrium settings.

*Model.* We model the chiral fluid as a system of  $N + 1$  interacting Brownian particles in two spatial dimensions. The chirality is encoded in the odd mobility  $\boldsymbol{\mu}_i$  for particle  $i \in \{0, \dots, N\}$ . Each particle is subjected to a constant external drift  $\mathbf{f}_i$ , such that the overdamped Langevin dynamics become

$$\dot{\mathbf{r}}_i(t) = \boldsymbol{\mu}_i \mathbf{f}_i - \boldsymbol{\mu}_i \sum_{j \neq i} \nabla_i U(\mathbf{r}_i, \mathbf{r}_j) + \boldsymbol{\eta}_i(t), \quad (2)$$

where  $U$  is the two-body interaction potential, effect-

ing in the interaction force  $-\sum_{j \neq i} \nabla_i U(\mathbf{r}_i, \mathbf{r}_j)$  on particle  $i$ . Note that the response to both, the external drift and the interaction force has transverse components encoded in  $\boldsymbol{\mu}_i$ .  $\boldsymbol{\eta}_i(t)$  is the driving Gaussian but nonwhite noise with mean  $\langle \boldsymbol{\eta}_i(t) \rangle = \mathbf{0}$  and correlation  $\langle \boldsymbol{\eta}_i(t) \boldsymbol{\eta}_j(t') \rangle = \mathbf{D}_i \delta_+(t-t') \delta_{ij} + \mathbf{D}_i^T \delta_-(t-t') \delta_{ij}$  [48, 49], where  $\mathbf{D}_i = D_{0,i}(\mathbf{1} + \kappa_i \boldsymbol{\epsilon})$  is the odd diffusion of particle  $i$ , analogous to Eq. (1). Here  $\delta_{\pm}(\cdot)$  represent variants of the Dirac delta distribution defined on the half-axis of the real numbers,  $\mathbb{R}_{\pm}$ , respectively [50]. For analytical simplicity, we assume a tensorial FDR, i.e.,  $\mathbf{D}_i = \boldsymbol{\mu}_i k_B T$ , where  $k_B T$  is the thermal energy. By tagging one particle, the tracer particle, we coarse-grain Eq. (2) over the interactions with the host particles in the limit of low density  $\phi \ll 1$  (see the Supplementary Material (SM) [51] for details). We adapt a geometric method in the coarsening [58, 59]. This allows us to analytically treat the oddness-affected probability fluxes, originating in the modified repulsive (so-called *oblique* [60]) boundary conditions introduced by the sterically interacting particles. The drift-diffusion equation for the one-body probability density function (PDF)  $p_t(\mathbf{x}, t)$ , to find the tracer in the interval  $[\mathbf{x}, \mathbf{x} + d\mathbf{x}]$  at time  $t$  becomes

$$\frac{\partial p_t(\mathbf{x}, t)}{\partial t} = \nabla \cdot [D \nabla - \mathbf{v}] p_t(\mathbf{x}, t). \quad (3)$$

Here  $D = \text{diag}(\mathbf{D}_t [1 - 4\phi \boldsymbol{\Gamma} \mathbf{D}_t])$  is the effective diffusion coefficient, where  $\boldsymbol{\Gamma} = (\mathbf{D}_t + \mathbf{D}_h) / \det(\mathbf{D}_t + \mathbf{D}_h)$ . The tracer drift  $\mathbf{v}$  is given by

$$\mathbf{v} = \boldsymbol{\mu}_{\text{dir}} \mathbf{f}_t + \boldsymbol{\mu}_{\text{indir}} \mathbf{f}_h, \quad (4)$$

where the mobilities

$$\boldsymbol{\mu}_{\text{dir}} = \boldsymbol{\mu}_t - 4\phi \mathbf{D}_t \boldsymbol{\Gamma} \boldsymbol{\mu}_t, \quad (5)$$

$$\boldsymbol{\mu}_{\text{indir}} = 4\phi \mathbf{D}_t \boldsymbol{\Gamma} \boldsymbol{\mu}_h, \quad (6)$$

are referred to as the *direct* and *indirect* mobility of the tracer particle, respectively. Here subscripts  $t$  and  $h$  refer to tracer and host particles, respectively.

Both,  $\boldsymbol{\mu}_{\text{dir}}$  and  $\boldsymbol{\mu}_{\text{indir}}$  are influenced by interactions between the tracer and host particles. In an ordinary, nonchiral fluid, these mobilities correspond to distinct physical scenarios; when only the tracer particle is driven ( $\mathbf{f}_h = \mathbf{0}$ ),  $\boldsymbol{\mu}_{\text{dir}}$  describes how the tracer advection is hindered by continuous collisions with the host particles at rest. Conversely, when the tracer remains at rest ( $\mathbf{f}_t = \mathbf{0}$ ), while the host particles are driven,  $\boldsymbol{\mu}_{\text{indir}}$  quantifies how the tracer is advected by the host particle stream, an effect mediated by interparticle interactions. In both cases, the tracer drifts in the direction of the applied force [61] (see also the SM [51]) a trend seen at all densities of the host particles. This intuitive behavior is reflected in the positivity of both transport coefficients, direct and indirect mobility. However, this is fundamentally different in a chiral fluid. We demonstrate that in a

chiral fluid with interacting particles these mobilities can turn negative leading to reversed tracer drift.

*Results.* We model the chiral fluid by fixing  $\boldsymbol{\mu}_t = \boldsymbol{\mu}_h$  and  $\mathbf{D}_t = \mathbf{D}_h$  and in particular  $\kappa_t = \kappa_h \equiv \kappa \neq 0$ . Despite this simplification, the model remains broadly applicable to describe systems with distinct particle responses, such as driven binary colloidal systems [62–64], and particularly tracer particles in chiral fluids [3, 6, 33, 34]. We first consider the case where the tracer particle and host particles are subjected to dragging forces parallel to each other along a direction, which we chose as the  $x$  direction, i.e.,  $\mathbf{f}_t = f_t \hat{\mathbf{e}}_x$  and  $\mathbf{f}_h = f_h \hat{\mathbf{e}}_x$ . As model parameters, we vary the magnitudes of the dragging forces. The results are shown for a chosen  $f_t$  and the ratio  $\tilde{f} = f_h/f_t$ . The drift of the tracer is decomposed into its components along and perpendicular to the tracer force, which are denoted by  $v_{\parallel}$  and  $v_{\perp}$ , respectively.

Consider the scenario in which  $f_t, f_h > 0$ , i.e., the chiral fluid and the tracer are dragged in the same direction. In contrast to the normal fluid, here the chiral tracer exhibits highly counterintuitive dynamics: for sufficiently large densities, the tracer’s drift velocity along the applied force reverses direction despite  $\tilde{f} > 0$ . The tracer drift becomes negative when the oddness exceeds a threshold  $\kappa > \kappa_{\text{rev}}^{\parallel}(\tilde{f}, \phi)$  that depends both on  $\tilde{f}$  and  $\phi$ , which need to obey  $\tilde{f} > 1 + 1/(6\phi)$  (for analytical details, see the SM [51]). The latter gives rise to a state diagram for negative tracer drift shown in Fig. 1(b) and we test the predictions against Brownian dynamics simulation results (see the SM [51] for details on simulations) for  $\tilde{f} = 3.77$  in Fig. 1(a). We observe three distinct regimes: at lower densities ( $\phi = 0.04$ ), the tracer exhibits ordinary drift, consistent with the applied force. At higher densities, in contrast, ( $\phi = 0.08$ ) the chiral tracer exhibits negative drift ( $v_{\parallel} < 0$ ). At the threshold density  $\phi = 0.06$ , the theory predicts an asymptotic negative drift as  $\kappa \rightarrow \infty$ . While the theory and simulations are in good agreement for small  $\kappa$  ( $\kappa \lesssim 2$ ), the measured effect is in fact much stronger than the theory predicts, compare Fig. 1(a).

To investigate the origin of the negative drift, we separately analyze the effects of direct and indirect mobility in Eq. (4) by either switching off the host or tracer drift as shown in the inset of Fig. 1(a). The direct mobility, which remains positive for all  $\kappa$  describes the normal drift response of the tracer in that it describes how the motion of a tracer is impeded due to interactions with host particles. The indirect mobility, in contrast, captures the enhancement of dynamics due to interactions with the chiral fluid. In other words, it is the response of the tracer to the driving of the host particles, which ultimately leads to a reversal of the tracer’s drift. The theory predicts a second regime with negative drift ( $\tilde{f} < 1 - 1/(2\phi)$ , i.e.,  $\tilde{f} < 0$  in the dilute region); see Fig. 1(b). Here, the tracer and host are dragged in opposite directions and thus, a reversal of tracer drift due to interactions might appear

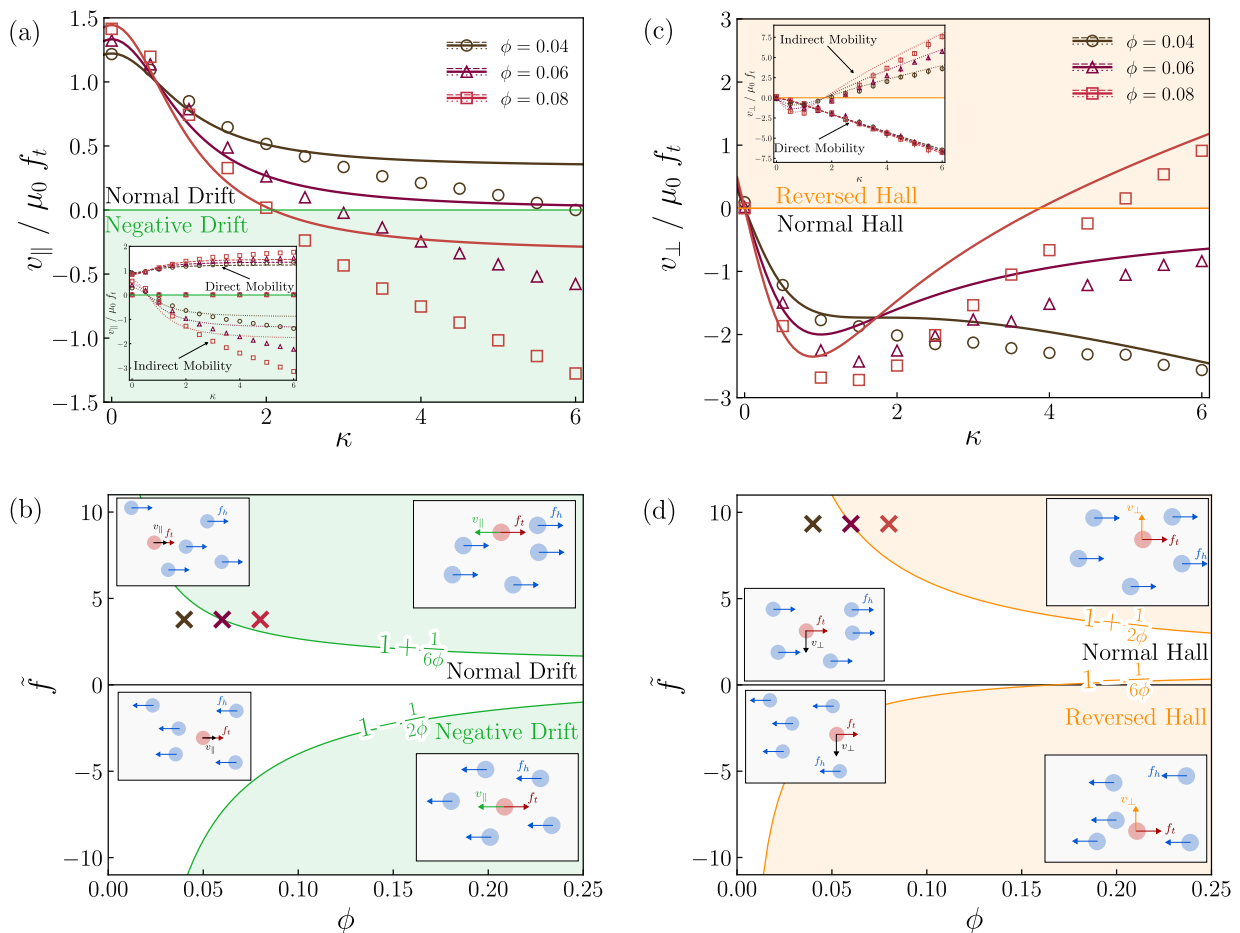


FIG. 1. *Reversal of tracer drift.* Components of the tracer drift  $\mathbf{v} = (v_{\parallel}, v_{\perp})$ , Eq. (4) (solid lines), of a driven chiral tracer in a driven chiral fluid. Symbols represent data from Brownian dynamics simulations. Error bars are smaller than the symbols. Tracer drift  $\mathbf{f}_t = f_t \hat{\mathbf{e}}_x$  and host drift  $\mathbf{f}_h = f_h \hat{\mathbf{e}}_x$  are taken to be parallel, the ratio of magnitudes  $\tilde{f} = f_h/f_t$  serves as a control parameter. (a) Tracer drift along the drift force  $v_{\parallel}$  as a function of odd mobility  $\kappa$  for  $\tilde{f} = 3.77$ . The densities  $\phi = 0.04, 0.06, 0.08$  correspond to the three regions of the state diagram (b) of normal drift, asymptotically negative drift, and negative drift (indicated by crosses). (c) Hall-drift of the tracer  $v_{\perp}$  as a function of odd mobility  $\kappa$  for  $\tilde{f} = 9.33$ . The densities  $\phi = 0.04, 0.06, 0.08$  correspond to the three regions of the state diagram (d) of ordinary Hall drift, asymptotic reversal, and reversal of Hall drift (indicated by crosses). Insets in (a) and (c) show the contribution of  $\mu_{\text{dir}}$  (dashed lines) and  $\mu_{\text{indir}}$  (dotted lines) according to Eqs. (5) and (6) to the negative drift and reversed Hall drift of the tracer. Sketches in (b) and (d) illustrate the tracer's drift in the respective region.

less surprising. More intriguingly, however, at sufficiently high oddness ( $\kappa > \kappa_{\text{rev}}^{\parallel}(\tilde{f}, \phi)$ ) the tracer overcomes the transferred effect of interactions and again follows the dragging force, despite the opposing host-particle stream.

We now focus on  $v_{\perp}$ , the tracer's drift velocity perpendicular to the applied force. From Eq. (4), we find that  $v_{\perp} \propto -\kappa$  in the absence of interactions, which corresponds to the characteristic Hall drift of a chiral tracer. In chiral fluids, interactions with the host particles can lead to a similarly counterintuitive effect as for  $v_{\parallel}$  and reverse the direction of  $v_{\perp}$  despite  $\tilde{f} > 0$  and  $\mathbf{f}_t \parallel \mathbf{f}_h$ . This is possible, if the chirality exceeds a threshold  $\kappa > \kappa_{\text{rev}}^{\perp}(\tilde{f}, \phi)$ , that depends both on  $\tilde{f}$  and  $\phi$ , which have to obey the relation  $\tilde{f} > 1 + 1/(2\phi)$  (for analytical details, see the SM [51]). The latter again gives rise to a

state diagram for reversed Hall drift, shown in Fig. 1(d). In Fig. 1(c) we demonstrate that for a chosen value of  $\tilde{f} = 9.33$ , in a system with sufficiently high density, the chiral tracer reverses its intrinsic Hall drift. Again three distinct regimes are found; at low densities ( $\phi = 0.04$ ), the tracer particle exhibits a Hall-like drift,  $v_{\perp} \propto -\kappa$ . However, at large densities ( $\phi = 0.08$ ), the Hall drift becomes non-monotonic as a function of  $\kappa$ , ultimately resulting in a reversal of the Hall drift ( $v_{\perp} > 0$ ). These regimes are separated by an asymptotically reversed Hall drift ( $\phi = 0.06$ ). Analogously to the negative drift, the reversal of Hall drift, thus, is induced by the indirect response of the tracer to the host driving in the

dilute limit. In fact, as evident from both state diagrams, Figs. 1(b) and (d), a reversal of the Hall drift necessarily accompanies a negative drift within the current setup and cannot occur independently.

The simultaneous reversal of both drift components is a direct consequence of the chosen setup, where the dragging forces are strictly parallel. A more general scenario is nonparallel drift forces, which have been thoroughly investigated, for example in driven colloidal systems [65, 66], in streamline flows [67] or in pedestrian dynamics [68–70]. With nonparallel forces, a broader range of tracer responses exists, allowing for control over its motion in all directions. For instance, Fig. 2 presents the state diagram and simulation results for a scenario in which  $\mathbf{f}_t$  is perpendicular to  $\mathbf{f}_h$ . In this case, the reversed Hall drift does not necessarily imply a negative drift, and both effects can be independently realized (see the SM for details [51]). The parallel and perpendicular dragging cases illustrate the essential nontrivial behavior of chiral fluids and their tunability. However, our theory provides a general prediction for an arbitrary angle between the tracer and host forces. This fully general response is analyzed in the SM [51].

*Discussion.* We demonstrated that the transport properties of a tracer in a chiral fluid exhibit rich and nontrivial behavior, strongly shaped by interparticle interactions with the host fluid. Driven chiral tracers can undergo a reversal of their intrinsic Hall drift and experience negative drift, emerging from the subtle interplay of chirality, particle density, and drift magnitude.

Our findings have significant experimental and theoretical implications for the rheological properties of chiral fluids, highlighting the fundamental role of interaction effects in shaping their transport phenomena. These insights are directly relevant for tracer dynamics in skyrmionic systems [71, 72], or bacterial suspensions [20–22], where our predictions can be experimentally tested. Additionally, our results may have implications for the sedimentation of chiral tracers [73, 74] with potentially different buoyancy than the (chiral) fluid [75–77]. Moreover, these results open up new research perspectives on how chirality influences collective behaviors, such as laning transitions in mixtures of oppositely driven species [62–64]. In these systems, spontaneous demixing occurs, leading to the formation of lanes with opposite flow.

Finally, we remark on the intriguing resemblance between absolute negative mobility [46, 47] and the negative drift observed in our system. This offers a fascinating example of a chiral fluid under flow acting as an engine, where the tracer, drifting opposite to the applied force, can perform work [78]. The fact that this phenomenon can already occur in a passive system challenges conventional perspectives on nonequilibrium transport and highlights the rich, unexplored dynamics of chiral fluids.

*Acknowledgments.* E. K., A. S., and R. M. acknowledge support by the Deutsche Forschungsgemeinschaft

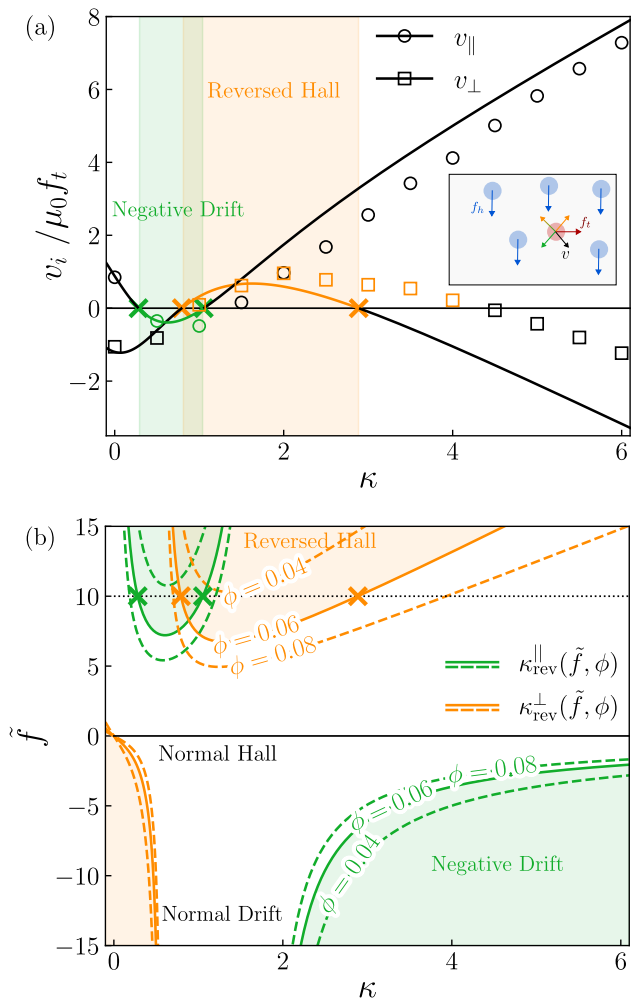


FIG. 2. *Orthogonal drift forces.* (a) Components  $v_i / \mu_0 f_t$  of the tracer drift  $\mathbf{v} = (v_{\parallel}, v_{\perp})$  from Eq (4) (solid lines), as a function of odd mobility  $\kappa$  for the case of tracer drift  $\mathbf{f}_t = f_t \hat{\mathbf{e}}_x$  perpendicular to host drift  $\mathbf{f}_h = -f_h \hat{\mathbf{e}}_y$  in a system with density  $\phi = 0.06$ . Symbols represent data from Brownian dynamics simulations. Error bars are smaller than the symbols. The ratio of magnitudes is chosen as  $\tilde{f} = f_h / f_t = 10$  and is indicated in the theoretical state diagram (b) by the dotted line. The state diagram shows that for different densities  $\phi = 0.04, 0.06, 0.08$  the reversed Hall drift (orange) and negative drift (green) can be realized independently or simultaneously. Crosses indicate the theoretically predicted on-, and offset of reversed drifts, and agree qualitatively well with simulations. Note that the choices of  $\tilde{f} > 0$  and  $\alpha = \arccos(\mathbf{f}_t \cdot \mathbf{f}_h) = -\pi/2$  is equivalent to  $\tilde{f} < 0$  and  $\alpha = \pi/2$  in (b).

(grants No. SPP 2332- 492009952, SH 1275/5-1 and ME 1535/16-1). S. R. acknowledges support by Deutscher Akademischer Austauschdienst (grant No. 57693453).

\* These two authors contributed equally

- <sup>†</sup> Corresponding author; [rmetzler@uni-potsdam.de](mailto:rmetzler@uni-potsdam.de)
- <sup>‡</sup> Corresponding author; [abhinav.sharma@uni-a.de](mailto:abhinav.sharma@uni-a.de)
- [1] N. H. P. Nguyen, D. Klotsa, M. Engel, and S. C. Glotzer, *Phys. Rev. Lett.* **112**, 075701 (2014).
- [2] E. Perez Ipiña, S. Otte, R. Pontier-Bres, D. Czerucka, and F. Peruani, *Nat. Phys.* **15**, 610 (2019).
- [3] Q. Yang, H. Zhu, P. Liu, R. Liu, Q. Shi, K. Chen, N. Zheng, F. Ye, and M. Yang, *Phys. Rev. Lett.* **126**, 198001 (2021).
- [4] C. B. Caporusso, G. Gonnella, and D. Levis, *Phys. Rev. Lett.* **132**, 168201 (2024).
- [5] E. Kalz, H. D. Vuijk, I. Abdoli, J.-U. Sommer, H. Löwen, and A. Sharma, *Phys. Rev. Lett.* **129**, 090601 (2022).
- [6] C. J. O. Reichhardt and C. Reichhardt, *Europhys. Lett.* **137**, 66004 (2022).
- [7] F. Ghimenti, L. Berthier, G. Szamel, and F. van Wijland, *Phys. Rev. Lett.* **131**, 257101 (2023).
- [8] D. Schick, M. Weißenhofer, L. Rózsa, J. Rothörl, P. Virnau, and U. Nowak, *Phys. Rev. Res.* **6**, 013097 (2024).
- [9] R. E. Troncoso and Á. S. Núñez, *Ann. Phys.* **351**, 850 (2014).
- [10] C. Reichhardt, D. Ray, and C. J. O. Reichhardt, *Phys. Rev. Lett.* **114**, 217202 (2015).
- [11] F. Büttner, I. Lemesh, and G. S. D. Beach, *Sci. Rep.* **8**, 4464 (2018).
- [12] R. Gruber, M. A. Brems, J. Rothörl, T. Sparmann, M. Schmitt, I. Kononenko, F. Kammerbauer, M.-A. Syskaki, O. Farago, P. Virnau, and M. Kläui, *Adv. Mater.* **35**, 2208922 (2023).
- [13] V. Soni, E. S. Bililign, S. Magkiriadou, S. Sacanna, D. Bartolo, M. J. Shelley, and W. T. M. Irvine, *Nat. Phys.* **15**, 1188 (2019).
- [14] H. Massana-Cid, D. Levis, R. J. H. Hernández, I. Pagonabarraga, and P. Tierno, *Phys. Rev. Res.* **3**, L042021 (2021).
- [15] E. S. Bililign, F. Balboa Usabiaga, Y. A. Ganan, A. Poncet, V. Soni, S. Magkiriadou, M. J. Shelley, D. Bartolo, and W. T. M. Irvine, *Nat. Phys.* **18**, 212 (2022).
- [16] B. A. Grzybowski, H. A. Stone, and G. M. Whitesides, *Nature* **405**, 1033 (2000).
- [17] W. Wang, G. Gardi, P. Maggaretti, V. Kishore, L. Koens, D. Son, H. Gilbert, Z. Wu, P. Harwani, E. Lauga, *et al.*, *Sci. Adv.* **8**, eabk0685 (2022).
- [18] W. R. DiLuzi, L. Turner, M. Mayer, P. Garstecki, D. B. Weibel, H. C. Berg, and G. M. Whitesides, *Nature* **435**, 1271 (2005).
- [19] E. Lauga, W. R. DiLuzi, G. M. Whitesides, and H. A. Stone, *Biophys. J.* **90**, 400 (2006).
- [20] K. Beppu, Z. Izri, T. Sato, Y. Yamanishi, Y. Sumino, and Y. T. Maeda, *Proc. Natl. Acad. Sci. USA* **118**, e2107461118 (2021).
- [21] A. P. Petroff, X.-L. Wu, and A. Libchaber, *Phys. Rev. Lett.* **114**, 158102 (2015).
- [22] H. Li, H. Chaté, M. Sano, X.-q. Shi, and H. Zhang, *Phys. Rev. X* **14**, 041006 (2024).
- [23] T. H. Tan, A. Mietke, J. Li, Y. Chen, H. Higinbotham, P. J. Foster, S. Gokhale, J. Dunkel, and N. Fakhri, *Nature* **607**, 287 (2022).
- [24] I. H. Riedel, K. Kruse, and J. Howard, *Science* **309**, 300 (2005).
- [25] P. Chen, S. Weady, S. Atis, T. Matsuzawa, M. J. Shelley, and W. T. Irvine, *Nat. Phys.* **21**, 146 (2024).
- [26] H. Kähler, J. Carstensen, M. Bonitz, H. Löwen, F. Greiner, and A. Piel, *Phys. Rev. Lett.* **109**, 155003 (2012).
- [27] A. Shalchi, *Space Sci. Rev.* **216**, 23 (2020).
- [28] J. E. Avron, *J. Stat. Phys.* **92**, 543 (1998).
- [29] D. Banerjee, A. Souslov, A. G. Abanov, and V. Vitelli, *Nat. Commun.* **8**, 1573 (2017).
- [30] A. Souslov, K. Dasbiswas, M. Fruchart, S. Vaikuntanathan, and V. Vitelli, *Phys. Rev. Lett.* **122**, 128001 (2019).
- [31] M. Fruchart, C. Scheibner, and V. Vitelli, *Annu. Rev. Condens. Matter Phys.* **14**, 471 (2023).
- [32] Y. Hosaka, R. Golestanian, and A. Vilfan, *Phys. Rev. Lett.* **131**, 178303 (2023).
- [33] C. Reichhardt and C. J. O. Reichhardt, *Phys. Rev. E* **100**, 012604 (2019).
- [34] A. R. Poggioli and D. T. Limmer, *Phys. Rev. Lett.* **130**, 158201 (2023).
- [35] C. Hargus, J. M. Epstein, and K. K. Mandadapu, *Phys. Rev. Lett.* **127**, 178001 (2021).
- [36] E. Kalz, H. D. Vuijk, J.-U. Sommer, R. Metzler, and A. Sharma, *Phys. Rev. Lett.* **132**, 057102 (2024).
- [37] The existence of antisymmetric isotropic tensors depends on the decomposition of tensor spaces into irreducible representations of the rotation group  $SO(d)$  in  $d$  dimensions. In  $d = 2$ , the antisymmetric part of a rank-2 tensor transforms as a pseudoscalar under  $SO(2)$  and remains isotropic. In  $d = 3$ , it transforms as an axial vector under  $SO(3)$  and is not invariant under all rotations, making it incompatible with isotropy [38].
- [38] H. Weyl, *The Classical Groups: Their Invariants and Representations*, 2nd ed. (Princeton University Press, 1946).
- [39] J. E. Avron, R. Seiler, and P. G. Zograf, *Phys. Rev. Lett.* **75**, 697 (1995).
- [40] L. V. Delacrétaz and A. Gromov, *Phys. Rev. Lett.* **119**, 226602 (2017).
- [41] T. Holder, R. Queiroz, and A. Stern, *Phys. Rev. Lett.* **123**, 106801 (2019).
- [42] K. Litzius, I. Lemesh, B. Krüger, P. Bassirian, L. Caretta, K. Richter, F. Büttner, K. Sato, O. A. Tretiakov, J. Förster, R. M. Reeve, M. Weigand, I. Bykova, H. Stoll, G. Schütz, G. S. D. Beach, and M. Kläui, *Nat. Phys.* **13**, 170 (2017).
- [43] W. Jiang, X. Zhang, G. Yu, W. Zhang, X. Wang, M. Benjamin Jungfleisch, J. E. Pearson, X. Cheng, O. Heinonen, K. L. Wang, Y. Zhou, A. Hoffmann, and S. G. E. te Velthuis, *Nat. Phys.* **13**, 162 (2017).
- [44] R. Lier, C. Duclut, S. Bo, J. Armas, F. Jülicher, and P. Surówka, *Phys. Rev. E* **108**, L023101 (2023).
- [45] X. Cao, D. Das, N. Windbacher, F. Ginot, M. Krüger, and C. Bechinger, *Nat. Phys.* **19**, 1904 (2023).
- [46] R. Eichhorn, P. Reimann, and P. Hänggi, *Phys. Rev. Lett.* **88**, 190601 (2002).
- [47] R. Eichhorn, P. Reimann, and P. Hänggi, *Phys. Rev. E* **66**, 066132 (2002).
- [48] H.-M. Chun, X. Durang, and J. D. Noh, *Phys. Rev. E* **97**, 032117 (2018).
- [49] J.-M. Park and H. Park, *Phys. Rev. Res.* **3**, 043005 (2021).
- [50]  $\delta_{\pm}(\cdot)$  are defined as variants of the Dirac delta distribution via  $\int_0^{\infty} du \delta_+(u) = \int_{-\infty}^0 du \delta_-(u) = 1$  and  $\int_{-\infty}^0 du \delta_+(u) = \int_0^{\infty} du \delta_-(u) = 0$  [48].
- [51] See Supplemental Material at `** *link * **` in which we

provide detailed information about the analytical model to account for interparticle interactions in chiral fluids in Section I, we demonstrate the explicit expression used in this manuscript in Section II, and provide detailed information about the Brownian dynamics simulations in Section III. The Supplementary Material further includes Refs. [52–57] which are not already in the paper.

- [52] Hänggi, *Z. Phys. B* **31**, 407 (1978).
- [53] H. Risken, *The Fokker-Planck Equation*, 2nd ed. (Springer Berlin, Heidelberg, 1989).
- [54] P. Hänggi and P. Jung, *Adv. Chem. Phys.* **89**, 239 (1995).
- [55] C. M. Bender and S. A. Orszag, *Advanced Mathematical Methods for Scientists and Engineers I* (Springer New York, 1999).
- [56] C. Gardiner, *Stochastic Methods*, 4th ed. (Springer-Verlag Berlin Heidelberg, 2009).
- [57] E. Kalz, *Diffusion under the Effect of Lorentz Force* (Springer Spektrum Wiesbaden, 2022).
- [58] M. Bruna and S. J. Chapman, *J. Chem. Phys.* **137**, 204116 (2012).
- [59] M. Bruna and S. J. Chapman, *Phys. Rev. E* **85**, 011103 (2012).
- [60] D. Gilbarg and N. S. Trudinger, *Elliptic Partial Differential Equations of Second Order*, 2nd ed. (Springer Berlin, Heidelberg, 2001).
- [61] J.-P. Hansen and I. R. McDonald, *Theory of Simple Liquids: With Applications to Soft Matter*, 4th ed. (Academic Press, 2013).
- [62] D. Helbing, I. J. Farkas, and T. Vicsek, *Phys. Rev. Lett.* **84**, 1240 (2000).
- [63] J. Dzubiella, G. P. Hoffmann, and H. Löwen, *Phys. Rev. E* **65**, 021402 (2002).
- [64] A. Poncet, O. Bénichou, V. Démery, and G. Oshanin, *Phys. Rev. Lett.* **118**, 118002 (2017).
- [65] J. Dzubiella and H. Löwen, *J. Phys. Condens. Matter* **14**, 9383 (2002).
- [66] J. Cividini, C. Appert-Rolland, and H. J. Hilhorst, *Europhys. Lett.* **102**, 20002 (2013).
- [67] S. Shin, J. T. Ault, P. B. Warren, and H. A. Stone, *Phys. Rev. X* **7**, 041038 (2017).
- [68] D. Helbing, L. Buzna, A. Johansson, and T. Werner, *Transp. Sci.* **39**, 1 (2005).
- [69] P. Mullick, S. Fontaine, C. Appert-Rolland, A.-H. Olivier, W. H. Warren, and J. Pettré, *PLoS Comput. Biol.* **18**, e1010210 (2022).
- [70] K. A. Bacik, B. S. Bacik, and T. Rogers, *Science* **379**, 923 (2023).
- [71] X. Zhang, J. Xia, O. A. Tretiakov, M. Ezawa, G. Zhao, Y. Zhou, X. Liu, and M. Mochizuki, *Phys. Rev. B* **108**, 144428 (2023).
- [72] K. Raab, M. Schmitt, M. A. Brems, J. Rothörl, F. Kammerbauer, S. Krischna, M. Kläui, and P. Virnau, *Phys. Rev. E* **110**, L042601 (2024).
- [73] N. W. Krapf, T. A. Witten, and N. C. Keim, *Phys. Rev. E* **79**, 056307 (2009).
- [74] E. Huseby, J. Gissinger, F. Candelier, N. Pujara, G. Verhille, B. Mehlig, and G. Voth, *Phys. Rev. Fluid.* **10**, 024101 (2025).
- [75] I. H. Herron, S. H. Davis, and F. P. Bretherton, *J. Fluid Mech.* **68**, 209 (1975).
- [76] J. Singh, A. E. Patteson, B. O. T. Maldonado, P. K. Purohit, and P. E. Arratia, *Soft Matter* **17**, 4151 (2021).
- [77] T. Khain, C. Scheibner, M. Fruchart, and V. Vitelli, *J. Fluid Mech.* **934**, A23 (2022).
- [78] P. Hänggi and F. Marchesoni, *Rev. Mod. Phys.* **81**, 387 (2009).

# Supplementary Material: Reversal of tracer advection and Hall drift in an interacting chiral fluid

Erik Kalz,<sup>1,\*</sup> Shashank Ravichandir,<sup>2,3,\*</sup> Johannes Birkenmeier,<sup>1</sup> Ralf Metzler,<sup>1,4,†</sup> and Abhinav Sharma<sup>2,5,‡</sup>

<sup>1</sup>University of Potsdam, Institute of Physics and Astronomy, D-14476 Potsdam, Germany

<sup>2</sup>Leibniz-Institute for Polymer Research, Institute Theory of Polymers, D-01069 Dresden, Germany

<sup>3</sup>Technical University of Dresden, Institute for Theoretical Physics, D-01069 Dresden, Germany

<sup>4</sup>Asia Pacific Centre for Theoretical Physics, KR-37673 Pohang, Republic of Korea

<sup>5</sup>University of Augsburg, Institute of Physics, D-86159 Augsburg, Germany

In this Supplementary Material, we provide the analytical and simulation background for the relations and figures shown in the main manuscript. In Section I, we present the theory for obtaining an effective drift-diffusion equation for a driven chiral tracer in a dilute suspension of driven chiral host particles. In Section IA we present the setup of overdamped chiral particles, where the chirality is encoded in odd transport tensors. In Section IB, we outline the derivation of an interaction-corrected drift-diffusion equation and specify the model in Section IC to the tracer and host model for chiral particles.

In Section II, we specify the generic model to the chiral fluid and present the relations to which we refer in the main manuscript. In Section IIA we present the main setup of this study, parallel tracer and host drift forces and in Section IIB the case of orthogonal drift forces. Section IIC demonstrates that our model also captures other scenarios such as the nonchiral tracer particle in a chiral fluid, widely investigated in the literature, as well as that it reduces to the ordinary nonchiral tracer in a nonchiral fluid as demonstrated in Section IID.

Finally, in Section III we give details on the Brownian dynamics simulations.

## CONTENTS

I. Modeling interacting chiral systems	1
A. Setup	1
B. Interactions in the dilute limit	2
C. Tracer and host model	3
II. The driven chiral fluid	3
A. Parallel drift forces	3
B. Orthogonal drift forces	4
C. Nonchiral tracer in chiral bath	5
D. Nonchiral tracer in nonchiral bath	5
III. Simulation Details	6
A. Parameters	6

\* These two authors contributed equally

† Corresponding author; [rmetzler@uni-potsdam.de](mailto:rmetzler@uni-potsdam.de)

‡ Corresponding author; [abhinav.sharma@uni-a.de](mailto:abhinav.sharma@uni-a.de)

## References

6

### I. MODELING INTERACTING CHIRAL SYSTEMS

#### A. Setup

Chiral fluids under drift are characterized by a Hall effect, i.e., a drift causes a response in the transverse direction [1]. On the level of tracer dynamics, and in a two-dimensional system, this is encoded in the *odd mobility* tensor [2, 3], which is a second-rank isotropic transport tensor giving the tracer response on an applied force. It is given by

$$\boldsymbol{\mu} = \mu_0(\mathbf{1} + \kappa \boldsymbol{\epsilon}), \quad (1)$$

where  $\mathbf{1}$  is the identity tensor and  $\boldsymbol{\epsilon}$  is the fully antisymmetric Levi-Civita symbol in two dimensions ( $\epsilon_{xx} = \epsilon_{yy} = 0$  and  $\epsilon_{xy} = -\epsilon_{yx} = 1$ ).  $\mu_0$  is the bare mobility with  $[\mu_0] = \text{s/kg}$ , and  $\kappa$  is the characteristic odd mobility with  $[\kappa] = 1$ . If we consider, as a demonstrative example, a drift force in  $x$ -direction,  $\mathbf{f} = f\hat{\mathbf{e}}_x$ , the average response velocity of a particle in the overdamped regime becomes  $\langle \dot{\mathbf{r}} \rangle = \mu_0 f (\hat{\mathbf{e}}_x - \kappa \hat{\mathbf{e}}_y)$ . Thus, odd mobility encodes the characteristic Hall-like response ( $\propto -\kappa \hat{\mathbf{e}}_y$ ) of a chiral particle. A complete description of the overdamped chiral dynamics requires to specify the diffusion coefficient. We, therefore, assume that the system obeys a fluctuation-dissipation relation (FDR) of the form  $\mathbf{D} = k_B T \boldsymbol{\mu}$ . Such behavior is known as *odd-diffusion* in the literature [4–6] and characterizes the broken time-reversal symmetry of a chiral overdamped fluid.  $k_B T$  here is the thermal energy with  $k_B$  as the Boltzmann constant and  $T$  the temperature of the medium.

We specifically want to investigate the effects of interparticle interactions on the transport properties of the chiral fluid. We, therefore, model the chiral fluid as an isotropic system of  $N$  interacting Brownian particles in two spatial dimensions. The overdamped Langevin equation for the position  $\mathbf{r}_i(t) \in \mathbb{R}^2$  of particle  $i \in \{1, \dots, N\}$  takes the form

$$\dot{\mathbf{r}}_i(t) = \boldsymbol{\mu}_i \mathbf{F}_i(\vec{\mathbf{r}}) + \boldsymbol{\eta}_i(t). \quad (2)$$

Here  $\mathbf{F}_i(\vec{\mathbf{r}}) = \mathbf{f}_i - \nabla_i U_N(\vec{\mathbf{r}})$  is the total force acting on particle  $i$ . It is composed of an external force  $\mathbf{f}_i(\mathbf{r}_i)$  acting on the position of particle  $i$  and the interaction force

$-\nabla_i U_N(\vec{\mathbf{r}})$  that stems from a generic  $N$ -body interaction potential  $U_N(\vec{\mathbf{r}})$ .  $\vec{\mathbf{r}} = (\mathbf{r}_1(t), \dots, \mathbf{r}_N(t))$  is the vector of all particle coordinates and  $\nabla_i$  the partial differential operator for the position of particle  $i$ . Each chiral particle  $i$  responds on the total force  $\mathbf{F}_i(\vec{\mathbf{r}})$  with an odd mobility of the form of Eq. (1),  $\boldsymbol{\mu}_i = \mu_0^{(i)}(\mathbf{1} + \kappa_i \boldsymbol{\epsilon})$ .

$\boldsymbol{\eta}_i(t)$  in Eq. (2) is a Gaussian noise, which has mean zero,  $\langle \boldsymbol{\eta}_i(t) \rangle = \mathbf{0}$ , and a nonwhite correlation  $\langle \boldsymbol{\eta}_i(t) \otimes \boldsymbol{\eta}_j(t') \rangle = \mathbf{D}_i \delta_+(t-t') \delta_{ij} + \mathbf{D}_i^T \delta_-(t-t') \delta_{ij}$  [7, 8].  $\mathbf{D}_i = D_0^{(i)}(\mathbf{1} + \kappa_i \boldsymbol{\epsilon})$  here is the odd diffusion tensor of particle  $i$  and  $(\cdot)^T$  denotes a matrix transpose.  $\delta_{\pm}(\cdot)$  represent variants of the Dirac delta distribution defined on the half-axis of the real numbers, i.e.,  $\int_0^\infty du \delta_+(u) = \int_{-\infty}^0 du \delta_-(u) = 1$  and  $\int_{-\infty}^0 du \delta_+(u) = \int_0^\infty du \delta_-(u) = 0$ . Further,  $\otimes$  denotes the outer product,  $(\mathbf{a} \otimes \mathbf{b})_{\alpha\beta} = a_\alpha b_\beta$  for some vectors  $\mathbf{a}$  and  $\mathbf{b}$  and Greek indices denoting components.

The non-white noise correlation implies that a corresponding probabilistic description to the Langevin dynamics in Eq. (2) cannot be derived using standard techniques [9, 10]. Using methods from (stochastic) functional calculus [11, 12], however, it is possible to derive the time-evolution equation for the probability density function (PDF), which also yields the correct probability flux, characterized by chirality-induced nonzero rotation as demonstrated in Refs. [7, 8]. The correct time-evolution equation for the  $N$ -body joint PDF,  $\mathcal{P}_N(t) = \mathcal{P}_N(\vec{\mathbf{x}}, t) = \left\langle \prod_{i=1}^N \delta(\mathbf{r}_i(t) - \mathbf{x}_i) \right\rangle_{\vec{\boldsymbol{\eta}}}$  to find each particle  $i$  within  $[\mathbf{x}_i, \mathbf{x}_i + d\mathbf{x}_i]$  at time  $t$  takes the form of  $\partial \mathcal{P}_N(t) / \partial t = -\sum_{i=1}^N \nabla_i \cdot \mathcal{J}_i(\vec{\mathbf{x}}, t)$ , where the diffusive flux  $\mathcal{J}_i(\vec{\mathbf{x}}, t)$  is given as

$$\mathcal{J}_i(\vec{\mathbf{x}}, t) = -[\mathbf{D}_i \nabla_i + \boldsymbol{\mu}_i \nabla_i U_N(\vec{\mathbf{x}}) - \boldsymbol{\mu}_i \mathbf{f}_i] P_N(\vec{\mathbf{x}}, t). \quad (3)$$

and thus has the characteristic, chirality-induced nonzero rotation,  $\nabla_i \wedge \mathcal{J}_i \propto \kappa_i$ , particularly in the diffusive part.

## B. Interactions in the dilute limit

We aim to derive the effect of interparticle interactions on the dynamical behavior of chiral particles. To gain analytical insight we restrict our analysis to the dilute limit, where the potential energy is assumed to be the sum of radial pair potentials  $U$ , i.e.,  $U_N(\mathbf{x}, t) = \sum_{i,j=1, i \neq j}^N U(x_{ij})$ , and  $x_{ij} = |\mathbf{x}_i - \mathbf{x}_j|$ . We further assume the interaction to be of the hard-disk nature, i.e., we assume an excluded volume condition for the particles of diameter  $d$ , i.e.,  $U(x_{ij}) = 0$  for  $x_{ij} \geq d$  or  $U(x_{ij}) = \infty$  for  $x_{ij} < d$  for any two particles  $i$  and  $j$ ,  $i \neq j$ .

The time-evolution equation for the joint two-body PDF  $\mathcal{P}_2(t) = \mathcal{P}_2(\mathbf{x}_1, \mathbf{x}_2, t)$  can be specified from Eq. (3) to be

$$\begin{aligned} \frac{\partial}{\partial t} \mathcal{P}_2(t) &= \nabla_1 \cdot [\mathbf{D}_1 \nabla_1 - \boldsymbol{\mu}_1 (\mathbf{f}_1 - \nabla_1 U(x_{12}))] \mathcal{P}_2(t) \\ &+ \nabla_2 \cdot [\mathbf{D}_2 \nabla_2 + \boldsymbol{\mu}_2 (\mathbf{f}_2 - \nabla_2 U(x_{12}))] \mathcal{P}_2(t). \end{aligned} \quad (4)$$

We are interested in deriving an effective time-evolution equation for the one-body PDF,  $p_1(\mathbf{x}_1, t)$ , of particle one, exemplarily, by integrating out particle two in Eq. (4). Formally,

$$\begin{aligned} p_1(\mathbf{x}_1, t) &= \int d\mathbf{x}_2 \mathcal{P}_2(\mathbf{x}_1, \mathbf{x}_2, t) \\ &= \int_{\mathbb{R}^2 \setminus B_d(\mathbf{x}_1)} d\mathbf{x}_2 P_2(\mathbf{x}_1, \mathbf{x}_2, t). \end{aligned} \quad (5)$$

Here we took advantage of the excluded volume condition of the hard-disk interaction by defining the two-particle joint PDF as  $\mathcal{P}_2(\mathbf{x}_1, \mathbf{x}_2, t) = \Theta(x_{12} - d) P_2(\mathbf{x}_1, \mathbf{x}_2, t)$ , where  $\Theta(\cdot)$  is the (left-sided) Heaviside step function.  $\mathbb{R}^2 \setminus B_d(\mathbf{x}_i)$  here denotes the reduced configuration space for particle two, given that particle one is at position  $\mathbf{x}_1$  and created the excluded volume of  $B_d(\mathbf{x}_1)$ . This reduced configuration space makes the integration over particle two nontrivial, as it creates an (inner) moving boundary that must be respected in the coarse-graining procedure. Originating in the excluded volume condition of the hard disks, the non-overlap condition of the hard-disk interaction translates into a no-flux condition for the probabilistic flux. Here the special nature of chirality has to be respected, as this extends the usual Neumann-boundary condition into a so-called oblique boundary condition [13]. This allows for an orthogonal flux, the mathematical representation of chirality of the particles.

The effective time-evolution equation for  $p_1(t) = p_1(\mathbf{x}_1, t)$  becomes [5, 14–16]

$$\frac{\partial}{\partial t} p_1(t) = \nabla_1 \cdot [\mathbf{D}_1 \nabla_1 - \boldsymbol{\mu}_1 \mathbf{f}_1] p_1(t) + I_{12}(\mathbf{x}_1, t), \quad (6)$$

where  $I_{12}(\mathbf{x}_1, t)$  encodes the two-body interaction contribution and is given by

$$I_{12}(\mathbf{x}_1, t) = - \int_{\partial B_d(\mathbf{x}_1)} dS_2 \mathbf{n}_2 \cdot [\mathbf{D}_1^T \nabla_1 + \mathbf{D}_1 \nabla_2] P_2(t). \quad (7)$$

Here  $dS_2 \mathbf{n}_2$  is the directed surface element of particle two.

To approximate  $I_{12}$  systematically in the two-body limit, we expand  $P_2(t)$  as a perturbation series in  $\sigma = d/L$ , where  $L$  is a typical length scale of the domain of diffusion, i.e.,  $P_2(t) = P_2^{(0)}(t) + \sigma P_2^{(1)}(t) + \mathcal{O}(\sigma^2)$  and insert that into Eq. (7). Given the local nature of the interaction between particles in space, the key idea is to divide space into regions where particles are either well-separated ( $|\mathbf{x}_1 - \mathbf{x}_2| \gg \sigma$ ) or closely interacting ( $|\mathbf{x}_1 - \mathbf{x}_2| \sim \sigma$ ).  $I_{12}$  is expected only to contribute in these interaction regions. Solutions in both regions are then matched using the method of asymptotic expansions [17]. Within the two-particle picture  $I_{12}$  can be evaluated exactly and becomes [16]

$$\begin{aligned} I_{12}(\mathbf{x}_1, t) &= \pi \sigma^2 \nabla_1 \cdot \mathbf{D}_1 [(\mathbf{1} + \Gamma \mathbf{D}_2) p_1 \nabla_1 p_2 \\ &- \Gamma \mathbf{D}_1 p_2 \nabla_1 p_1 + \Gamma (\boldsymbol{\mu}_1 \mathbf{f}_1 - \boldsymbol{\mu}_2 \mathbf{f}_2) p_1 p_2], \end{aligned} \quad (8)$$



where we have defined  $\mathbf{\Gamma} = (\mathbf{D}_1 + \mathbf{D}_2)/\det(\mathbf{D}_1 + \mathbf{D}_2)$ , and abbreviated  $p_1 = p_1(\mathbf{x}_1, t)$ ,  $p_2 = p_2(\mathbf{x}_1, t)$ . Note that  $P_2^{(0)}(t)$  does not contribute to  $I_{12}$ , as it represents the interaction-free contribution of the perturbation problem.

In the dilute limit, this model now can be extended to contain  $N_1$  particles of species one and  $N_2$  of species two with  $(N_1 + N_2)\sigma \ll 1$ .  $N_2 I_{12}$  thus represents the inter-species interaction contribution to Eq. (6). However, for a tracer particle of species one, there are also  $(N_1 - 1)$  intra-species interactions, which are not accounted for by  $I_{12}$  yet. They can be, however, included by considering a fictitious analog of Eq. (6), where all particle labels are replaced by those of particle one. It is thus possible, to derive the intra-species correction as  $(N_1 - 1) I_{11}$ . The time-evolution equation for  $p_1(\mathbf{x}, t)$  thus contains the interaction-free term, Eq. (6), inter-species interaction contributions, Eq. (8), and intra-species contributions.

### C. Tracer and host model

We specify the model to that of a tracer and a host species, i.e. we assign one species to describe the tracer particle,  $N_1 = 1$ , and the other species to describe the host particles  $N_2 = N$ , such that we have  $N_1 + N_2 = N + 1$  particles in total. We denote the tracer species by the subscript  $t$  and the host species by the subscript  $h$ , i.e.,  $p_1(t) \rightarrow p_t(t)$  and  $p_2(t) \rightarrow p_h(t)$ . We define where  $c = \pi\sigma^2/4$  as the area of a particle and  $\phi(\mathbf{x}, t) = Nc p_h(\mathbf{x}, t)$  as the area concentration of the host species. This, for large  $N$ , approximately equals the full area concentration of particles in the system.

We assume  $\phi(\mathbf{x}, t) = \phi$  as constant, and the diluteness assumption implies  $\phi \ll 1$ . The equation for  $p_t(t)$  can be brought into the form of a drift-diffusion equation for the tracer, which is reported in the main manuscript and reads

$$\frac{\partial p_t(\mathbf{x}, t)}{\partial t} = \nabla \cdot [D\nabla - \mathbf{v}(\mathbf{x})] p_t(\mathbf{x}, t), \quad (9)$$

where

$$D = \text{diag} \mathbf{D}_t [1 - 4\phi \mathbf{\Gamma} \mathbf{D}_t], \quad (10)$$

$$\mathbf{v}(\mathbf{x}) = \boldsymbol{\mu}_t \mathbf{f}_t(\mathbf{x}) - 4\phi \mathbf{D}_t \mathbf{\Gamma} (\boldsymbol{\mu}_t \mathbf{f}_t - \boldsymbol{\mu}_h \mathbf{f}_h), \quad (11)$$

are the diffusion coefficient and tracer drift, respectively.

## II. THE DRIVEN CHIRAL FLUID

We model a chiral fluid of all-identical chiral particles by  $\boldsymbol{\mu}_t = \boldsymbol{\mu}_h$  and  $\mathbf{D}_t = \mathbf{D}_h$  and in particular  $\kappa_t = \kappa_h \equiv \kappa \neq 0$ . Tracer and host particles are subjected to a drift,  $\mathbf{f}_t$ ,  $\mathbf{f}_h$ , respectively. If we were to consider equal drift of host and tracer particles, i.e.,  $\mathbf{f}_t = \mathbf{f}_h$ , it can be easily seen that Eq. (9) is Galileian invariant under the transformation  $\mathbf{x} \rightarrow \mathbf{x} - \mathbf{v}t$  and it becomes a pure (interaction-corrected) diffusion equation. To gain insight into the

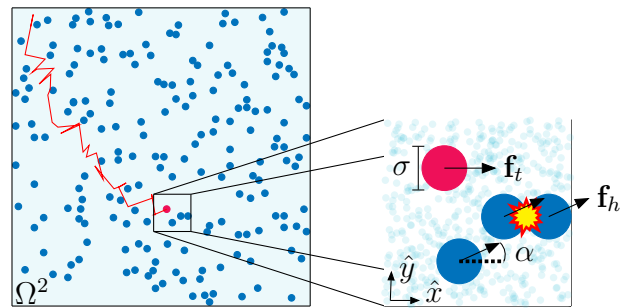


FIG. 1. *Sketch.* Schematic of a driven chiral fluid, where tracer (red) and host (blue) particles experience the drift forces  $\mathbf{f}_t$  and  $\mathbf{f}_h$ , respectively. The drift forces can be non-parallel in general, i.e.,  $\alpha = \arccos(\mathbf{f}_t \cdot \mathbf{f}_h) \in [-\pi/2, \pi/2]$ . The tracer particle is experiencing the ordinary Hall drift  $(\mathbf{v}_{\text{eff}})_y \propto -\kappa$ , which is curving the trajectory.

drift properties of a chiral tracer, it is, therefore, meaningful to consider a situation where  $\mathbf{f}_t \neq \mathbf{f}_h$ . We consider a situation of spatially constant drift and choose the coordinate system such that  $\mathbf{f}_t = f_t \hat{e}_x$ . The host-driving, thus, takes the general form of  $\mathbf{f}_h = f_h (\cos(\alpha), \sin(\alpha))^T$ ,  $\alpha \in [-\pi/2, \pi/2]$ . The ratio of drift magnitudes  $\tilde{f} = f_h/f_t$  serves as a control parameter. The tracer drift in Eq. (11) is decomposed along and perpendicular to the tracer force and is denoted by  $v_{\parallel}$  and  $v_{\perp}$ , respectively. It becomes

$$\begin{pmatrix} v_{\parallel} \\ v_{\perp} \end{pmatrix} = \mu_0 f_t \left[ \begin{pmatrix} 1 \\ -\kappa \end{pmatrix} - \frac{2\phi}{1 + \kappa^2} \begin{pmatrix} (1 - 3\kappa^2)(1 - \tilde{f} \cos(\alpha)) + \tilde{f} \sin(\alpha) \kappa(\kappa^2 - 3) \\ \kappa(\kappa^2 - 3)(1 - \tilde{f} \cos(\alpha)) - \tilde{f} \sin(\alpha)(1 - 3\kappa^2) \end{pmatrix} \right]. \quad (12)$$

An illustration of the setup can be seen in Fig. 1, and the rich interplay of chirality, density and drift forces for the tracer response can be seen in Fig. 2.

### A. Parallel drift forces

In the main manuscript, we prominently consider the situation of  $\mathbf{f}_t \parallel \mathbf{f}_h$ , i.e.,  $\alpha = 0$ . The tracer drift of Eq. (12)

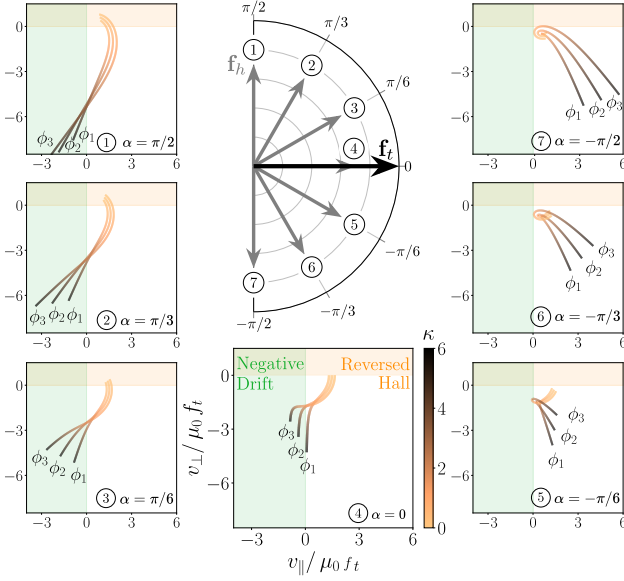


FIG. 2. *Nonparallel drift forces.* Each data point corresponds to the parallel and perpendicular drift  $(v_{\parallel}, v_{\perp})/\mu_0 f_t$  of the chiral tracer in a chiral host medium. For a given density and angle  $\alpha = \arccos(\mathbf{f}_t \cdot \mathbf{f}_h)$  between the tracer and host force, the curves show the variation of the drift velocities with varying  $\kappa$ . The tracer response becomes highly tunable. Shown are three different densities  $\phi_1 = 0.04$ ,  $\phi_2 = 0.06$  and  $\phi_3 = 0.08$  for a ratio of drift magnitudes  $\tilde{f} = f_h/f_t = 5$ . The situation  $\tilde{f} > 0$  and  $\alpha \in [-\pi/2, \pi/2]$  is equivalent to  $\tilde{f} < 0$  and  $\alpha \in [\pi/2, -\pi/2]$ .

specifies to

$$\begin{pmatrix} v_{\parallel} \\ v_{\perp} \end{pmatrix} = \mu_0 f_t \left[ \begin{pmatrix} 1 \\ -\kappa \end{pmatrix} - \frac{2\phi}{1 + \kappa^2} (1 - \tilde{f}) \begin{pmatrix} 1 - 3\kappa^2 \\ \kappa(\kappa^2 - 3) \end{pmatrix} \right]. \quad (13)$$

Negative tracer drift,  $v_{\parallel}/(\mu_0 f_t) < 0$ , becomes possible for  $\tilde{f} > 1 + 1/(6\phi)$  and  $\kappa > \kappa_{\text{rev}}^{\parallel}(\tilde{f}, \phi)$ , or  $\tilde{f} < 1 - 1/(2\phi)$  and  $0 < \kappa < \kappa_{\text{rev}}^{\parallel}(\tilde{f}, \phi)$ , where

$$\kappa_{\text{rev}}^{\parallel}(\tilde{f}, \phi) = \sqrt{\frac{1 + 2\phi(\tilde{f} - 1)}{6\phi(\tilde{f} - 1) - 1}}. \quad (14)$$

Note that the second condition  $\tilde{f} < 1 - 1/(2\phi)$  implies  $\tilde{f} < 0$  for  $\phi \in [0, 0.5)$ , the regime of validity of the model [14], implying that tracer and host particles are driven in opposite directions.

A reversal of the intrinsic Hall drift of the tracer,  $v_{\perp}/(\mu_0 f_t) > 0$ , becomes possible for  $\tilde{f} > 1 + 1/(2\phi)$  and  $\kappa > \kappa_{\text{rev}}^{\perp}(\tilde{f}, \phi)$ , or  $\tilde{f} < 1 - 1/(6\phi)$  and  $0 < \kappa < \kappa_{\text{rev}}^{\perp}(\tilde{f}, \phi)$ , where

$$\kappa_{\text{rev}}^{\perp}(\tilde{f}, \phi) = \sqrt{\frac{1 + 6\phi(\tilde{f} - 1)}{2\phi(\tilde{f} - 1) - 1}}. \quad (15)$$

Note that the second condition  $\tilde{f} < 1 - 1/(6\phi)$  implies  $\tilde{f} < 0$  for  $\phi \in [0, 0.17]$ , implying an opposite drift of tracer and host particles in the dilute regime.

As stated in the main manuscript, the negative tracer drift,  $v_{\parallel}/(\mu_0 f_t) < 0$ , amounts to an interpretation of absolute negative mobility (ANM) of the tracer. This interpretation can be strengthened by analyzing the power it takes to drag the tracer. The power is defined as  $P_{\text{trac}} = \mathbf{v} \cdot \mathbf{f}_t$ . In the system under consideration, it is given by

$$\frac{P_{\text{trac}}}{P_{\text{trac}}^{\phi=0}} = 1 - 2\phi(1 - \tilde{f}) \frac{1 - 3\kappa^2}{1 + \kappa^2}, \quad (16)$$

normalized by the power to drag the tracer in the absence of interactions  $P_{\text{trac}}^{\phi=0} = \mu_0 f_t^2$ . For  $\kappa > \kappa_{\text{rev}}^{\parallel}(\tilde{f}, \phi)$  and sufficiently large  $\tilde{f}$ , indeed  $P_{\text{trac}} < 0$  suggesting that the tracer can perform work against the drift force and thus resembles ANM, as shown in Fig. 3 (a). However, the negative tracer drift originates entirely from the interaction transferred response to the host driving and disappears in the limit of vanishing host drift  $\tilde{f} = f_h/f_t \rightarrow 0$ , as illuminated in the main manuscript. The distinction to ANM becomes even clearer when considering the total power to drag all particles  $P_{\text{tot}} = \mathbf{v} \cdot \mathbf{f}_t + N\mathbf{v}_h \cdot \mathbf{f}_h$ , which further includes the effective drift of the  $N$  host particles,  $\mathbf{v}_h$ . The latter can be obtained from an analog to Eq. (9). The total power reads

$$\frac{P_{\text{tot}}}{P_{\text{tot}}^{\phi=0}} = 1 - 2\phi \frac{(1 - \tilde{f})^2}{1 + N\tilde{f}^2} \frac{1 - 3\kappa^2}{1 + \kappa^2}, \quad (17)$$

where  $P_{\text{tot}}^{\phi=0} = \mu_0(f_t^2 + Nf_h^2)$  again is the total power in the absence of interactions. The relevant term  $(1 - \tilde{f})^2/(1 + N\tilde{f}^2)$  asymptotically approaches 1 for  $f_t \gg f_h$  and  $1/N \rightarrow 0$  for  $f_t \ll f_h$  and large  $N$ . Consequently, in the dilute limit ( $\phi \ll 1$ ),  $P_{\text{tot}}$  remains strictly positive as shown in Fig. 3 (b) and in agreement with the second law of thermodynamics [18, 19]. Particularly  $\kappa > 0$  only increases the total power to drag the particles.

## B. Orthogonal drift forces

In the main manuscript, we further consider the situation of orthogonal drift forces, i.e.,  $\alpha = \pm\pi/2$ . The tracer drift of Eq. (12) specifies to

$$\begin{pmatrix} v_{\parallel} \\ v_{\perp} \end{pmatrix} = \mu_0 f_t \left[ \begin{pmatrix} 1 \\ -\kappa \end{pmatrix} - \frac{2\phi}{1 + \kappa^2} \left( \begin{pmatrix} 1 - 3\kappa^2 \\ \kappa^3 - 3\kappa \end{pmatrix} - |\tilde{f}| \begin{pmatrix} \kappa^3 - 3\kappa \\ 3\kappa^2 - 1 \end{pmatrix} \right) \right]. \quad (18)$$

Note that the choice  $\tilde{f} < 0$  and  $\alpha = \pi/2$  is equivalent to  $\tilde{f} > 0$  and  $\alpha = -\pi/2$ . Solving for the threshold chirality for negative drift and reversed Hall drift of the tracer amounts for solving a third-order polynomial inequality. We, therefore, restrict ourselves to give relations for the state diagram.

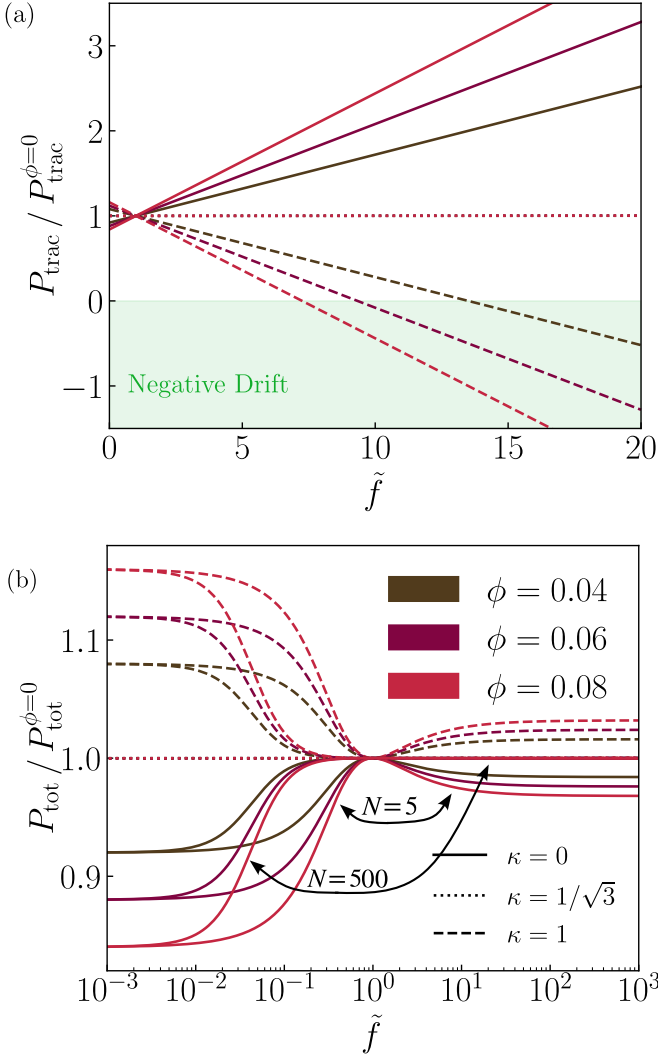


FIG. 3. *Power.* (a) Tracer power according to Eq. (16). (b) Total power according to Eq. (17) for two different numbers of total particles  $N + 1 = 6$  and  $N + 1 = 501$ . Both (a) and (b) share the same legends which coincides with the choices for  $\phi = 0.04, 0.06, 0.08$  of the main manuscript figures.

Negative tracer drift,  $v_{\parallel}/(\mu_0 f_t) < 0$ , becomes possible for  $\kappa > \sqrt{3}$  and  $\tilde{f} < \tilde{f}_{\text{rev}}^{\parallel}(\kappa, \phi)$ , or  $0 < \kappa < \sqrt{3}$  and  $\tilde{f} > \tilde{f}_{\text{rev}}^{\parallel}(\kappa, \phi)$ , where

$$\tilde{f}_{\text{rev}}^{\parallel}(\kappa, \phi) = \frac{1 + \kappa^2 - 2\phi(1 - 3\kappa^2)}{2\phi\kappa(3 - \kappa^2)}. \quad (19)$$

A reversal of the intrinsic Hall drift of the tracer,  $v_{\perp}/(\mu_0 f_t) > 0$ , becomes possible for  $\kappa > 1/\sqrt{3}$  and  $\tilde{f} > \tilde{f}_{\text{rev}}^{\perp}(\kappa, \phi)$ , or  $0 < \kappa < 1/\sqrt{3}$  and  $\tilde{f} < \tilde{f}_{\text{rev}}^{\perp}(\kappa, \phi)$ , where

$$\tilde{f}_{\text{rev}}^{\perp}(\kappa, \phi) = \frac{\kappa(1 + \kappa^2 - 2\phi(3 - \kappa^2))}{2\phi(3\kappa^2 - 1)}. \quad (20)$$

Eqs. (19) and (20) are plotted as the state diagram for different densities  $\phi = 0.04, 0.06, 0.08$  and as a function of  $\kappa$  in Fig. 2 of the main manuscript.

### C. Nonchiral tracer in chiral bath

The effective drift-diffusion equation (9) for the interaction-corrected dynamics of a tracer in a Brownian fluid can be analyzed for various setups. We further demonstrate a common choice in the literature: the nonchiral tracer in a chiral bath [2, 3, 20, 21]. This situation is modeled as  $\boldsymbol{\mu}_t = \mu_0 \mathbf{1}$  and  $\boldsymbol{\mu}_h = \mu_0(\mathbf{1} + \kappa_h \boldsymbol{\epsilon})$ , as well as  $\mathbf{D}_t = D_0 \mathbf{1}$  and  $\mathbf{D}_h = D_0(\mathbf{1} + \kappa_h \boldsymbol{\epsilon})$ . We again consider  $\mathbf{f}_t \parallel \mathbf{f}_h \propto \hat{\mathbf{e}}_x$  for demonstration purposes. For simplicity we chose equal bare mobility and bare diffusion among tracer and host particles, different choices are straightforward. For the exemplary setup of parallel drift forces, the effective tracer drift of Eq. (11) specifies to

$$\begin{pmatrix} v_{\parallel} \\ v_{\perp} \end{pmatrix} = \mu_0 f_t \begin{bmatrix} 1 \\ 0 \end{bmatrix} - \frac{4\phi}{4 + \kappa_h^2} \begin{pmatrix} 2 - \tilde{f}(2 - \kappa_h^2) \\ \kappa_h(3\tilde{f} - 1) \end{pmatrix}. \quad (21)$$

Notably, and in accordance with the literature, the nonchiral tracer adopts the characteristic Hall drift via interactions with the chiral host medium,  $v_{\perp} \propto -\phi \kappa_h$ .

A similar analysis as before can be performed and we see negative tracer drift,  $v_{\parallel}/(\mu_0 f_t) < 0$ , for  $\tilde{f} > 1/(4\phi)$  and  $\kappa_h > \kappa_{\text{rev},h}^{\parallel}(\tilde{f}, \phi)$ , or  $\tilde{f} < 1 - 1/(2\phi)$  and  $0 < \kappa_h < \kappa_{\text{rev},h}^{\parallel}(\tilde{f}, \phi)$ , where

$$\kappa_{\text{rev},h}^{\parallel}(\tilde{f}, \phi) = 2\sqrt{\frac{2\phi(1 - \tilde{f}) - 1}{1 - 4\phi\tilde{f}}}. \quad (22)$$

The condition for the reversal of (interaction-induced) Hall-drift,  $v_{\perp}/(\mu_0 f_t) > 0$ , reads  $\tilde{f} > 1/3$ .

We leave further analysis and validation of these predictions for future work.

### D. Nonchiral tracer in nonchiral bath

We finally provide the analytical predictions for the nonchiral tracer in the nonchiral fluid, i.e., the classical reference situation. Here  $\kappa_t = \kappa_h = 0$  in particular and we consider the situation where  $\boldsymbol{\mu}_t = \boldsymbol{\mu}_h = \mu_0 \mathbf{1}$  and  $\mathbf{D}_h = \mathbf{D}_t = D_0 \mathbf{1}$ . Again, we chose equal bare mobility and diffusion among tracer and host particles for simplicity, different choices are straightforward. The effective tracer drift of Eq. (11) specifies to

$$\begin{pmatrix} v_{\parallel} \\ v_{\perp} \end{pmatrix} = \mu_0 f_t \begin{bmatrix} 1 \\ 0 \end{bmatrix} - 2\phi \begin{pmatrix} 1 - \tilde{f}\cos(\alpha) \\ -\tilde{f}\sin(\alpha) \end{pmatrix}. \quad (23)$$

In the absence of chirality, both for the tracer and the host particles, there is no Hall drift,  $v_{\perp}|_{\phi=0} = 0$ . However, for  $\alpha \neq 0$  and the host particles being driven in a different direction than the tracer particle, interparticle interactions transfer an orthogonal drift  $\propto \phi \sin(\alpha)$  onto the tracer, i.e., the projected component of the non-aligned host drift. The tracer further shows an intuitive drift behavior in  $v_{\parallel}$ ; for  $f_t < f_h$  the tracer drift

gets enhanced by interactions,  $v_{\parallel} > v_{\parallel}|_{\phi=0}$ , as the host crowd is subjected to a stronger drift. For  $f_t > f_h$ , on the contrary, collisions with the slower host species impede the tracer drift and  $v_{\parallel} < v_{\parallel}|_{\phi=0}$ . There is, however, a formal situation of negative tracer drift for  $\tilde{f} < 1 - 1/(2\phi) < 0$  in  $\phi \in [0, 0.5)$ . This situation corresponds to the tracer particle being driven in the opposite direction of the host particles. If the tracer is driven with  $f_t < -f_h 2\phi/(2\phi - 1)$ , it still follows the opposite host-particle stream and thus, formally, responds negatively on its applied drift.

### III. SIMULATION DETAILS

The simulations for this system are done in two dimensions. The Langevin equations for disk  $i \in \{1, \dots, N\}$  used for the simulations are

$$\frac{\partial \mathbf{r}_i}{\partial t} = \mathbf{v}_i, \quad (24)$$

$$\frac{\partial \mathbf{v}_i}{\partial t} = -\frac{\gamma_i}{m_i}(\mathbf{1} - \kappa_i \boldsymbol{\epsilon})\mathbf{v}_i + \frac{1}{m_i}\mathbf{F}_i + \frac{1}{m_i}\boldsymbol{\zeta}_i. \quad (25)$$

Here  $\gamma_i$ ,  $m_i$ , and  $\kappa_i$  are the friction coefficient, mass and oddness of particle  $i$ ,  $\boldsymbol{\epsilon}$  is the two-dimensional Levi-Civita symbol and  $\boldsymbol{\zeta}_i$  is a zero-mean Gaussian white noise accounting for the fluctuations  $\langle \boldsymbol{\zeta}_i(t)\boldsymbol{\zeta}_j^T(t') \rangle = 2\gamma_i T \mathbf{1} \delta_{ij} \delta(t - t')$ , where the normalized temperature  $T$  is such that the Boltzmann constant is unity.  $\mathbf{F}_i$  is the total force experienced by particle  $i$  and given by

$$\mathbf{F}_i = \mathbf{f}_i + \sum_{j=1, i \neq j}^N \mathbf{f}_{ij}, \quad (26)$$

where  $\mathbf{f}_i$  is the external force acting on the disk:  $\mathbf{f}_i = \mathbf{f}_h$  if particle  $i$  belong to the host species and  $\mathbf{f}_i = \mathbf{f}_t$  for the tracer particle.  $\mathbf{f}_{ij}$  is the force acting on particle  $i$  due to

interaction with particle  $j$  and is given by

$$\mathbf{f}_{ij} = \begin{cases} \varepsilon \left( \frac{\sigma}{|\mathbf{r}_{ij}|} \right)^\alpha \mathbf{r}_{ij}, & \text{if } |\mathbf{r}_{ij}| < \sigma_c \\ 0, & \text{otherwise,} \end{cases} \quad (27)$$

where  $\mathbf{r}_{ij} = \mathbf{r}_i - \mathbf{r}_j$ ,  $\sigma$  is the diameter of the particles,  $\varepsilon$  is the energy scale of the potential,  $\alpha$  and  $\sigma_c$  are the steepness and the range of the potential, respectively.

#### A. Parameters

The simulations were carried out in a square box of length  $L$ , which was determined by the volume fraction  $\phi$  as  $L = \sqrt{\pi(N-1)/(4\phi)}$ . The total number of particles was set to  $N = 100$ , with  $N - 1$  host particles and one tracer particle. The temperature of the system is set to  $T = 1$ . The simulations were done with all particles having the same friction coefficient  $\gamma$  and oddness  $\kappa$ . The friction coefficient is  $\gamma = \gamma_0/(1 + \kappa^2)$  where  $\gamma_0 = 1$ . This normalization is done to keep the norm of the friction matrix  $\gamma(\mathbf{1} - \kappa \boldsymbol{\epsilon})$  unchanged with oddness and prevent energy dissipation. The mass of the particles is  $m = m_0/(1 + \kappa^2)$  and  $m_0$  was chosen to be  $10^{-2}$  such that  $m/\gamma = m_0/\gamma_0 = 10^{-2}$ . The parameters to mimic the hard potential were set to  $\sigma = 1$ ,  $\sigma_c = 1.01$ ,  $\varepsilon = 100$ , and  $\alpha = 17$ . The external forces in the system were set to  $\mathbf{f}_t = f_t \hat{\mathbf{e}}_x$  and  $\mathbf{f}_h = f_h \hat{\mathbf{e}}_y$  in Figs. 1(a) and (c) in the main text and  $\mathbf{f}_t = f_t \hat{\mathbf{e}}_x$  and  $\mathbf{f}_h = -f_h \hat{\mathbf{e}}_y$  in Fig. 2(a) in the main text. The  $f_t$  values were specified and  $f_h$  was calculated based on the desired force ratio  $\tilde{f} = f_h/f_t$ . We used  $f_t = 0.05$  for Figs. 1(c) and 2(b), and  $f_t = 0.5$  for Fig. 1(a) owing to the smaller value of  $\tilde{f}$  there.

The stochastic equations (24) and (25) were numerically integrated using the forward Euler method [5] with the timestep  $\Delta t = 10^{-5}$ . The trajectory of the tracer was studied by tracking the particle's position every  $10^5$  timesteps. The drift velocity components of the tracer were then obtained by fitting a straight line in the  $x$  vs.  $t$  and  $y$  vs.  $t$  data, respectively, and calculating the slopes. We performed 100 realizations of such simulations with trajectory length of  $t = 10^3$  with different random numbers and show the means of these 100 slopes as the data points in the plots.

- 
- [1] J. E. Avron, R. Seiler, and P. G. Zograf, *Phys. Rev. Lett.* **75**, 697 (1995).  
[2] C. J. O. Reichhardt and C. Reichhardt, *Europhys. Lett.* **137**, 66004 (2022).  
[3] A. R. Poggioli and D. T. Limmer, *Phys. Rev. Lett.* **130**, 158201 (2023).  
[4] C. Hargus, J. M. Epstein, and K. K. Mandadapu, *Phys. Rev. Lett.* **127**, 178001 (2021).  
[5] E. Kalz, H. D. Vuijk, I. Abdoli, J.-U. Sommer, H. Löwen, and A. Sharma, *Phys. Rev. Lett.* **129**, 090601 (2022).  
[6] E. Kalz, H. D. Vuijk, J.-U. Sommer, R. Metzler, and A. Sharma, *Phys. Rev. Lett.* **132**, 057102 (2024).  
[7] H.-M. Chun, X. Durang, and J. D. Noh, *Phys. Rev. E* **97**, 032117 (2018).  
[8] J.-M. Park and H. Park, *Phys. Rev. Res.* **3**, 043005 (2021).  
[9] C. Gardiner, *Stochastic Methods*, 4th ed. (Springer-Verlag Berlin Heidelberg, 2009).  
[10] H. Risken, *The Fokker-Planck Equation*, 2nd ed. (Springer Berlin, Heidelberg, 1989).  
[11] Hänggi, *Z. Phys. B* **31**, 407 (1978).  
[12] P. Hänggi and P. Jung, *Adv. Chem. Phys.* **89**, 239 (1995).

- [13] D. Gilbarg and N. S. Trudinger, *Elliptic Partial Differential Equations of Second Order*, 2nd ed. (Springer Berlin, Heidelberg, 2001).
- [14] M. Bruna and S. J. Chapman, *J. Chem. Phys.* **137**, 204116 (2012).
- [15] M. Bruna and S. J. Chapman, *Phys. Rev. E* **85**, 011103 (2012).
- [16] E. Kalz, *Diffusion under the Effect of Lorentz Force* (Springer Spektrum Wiesbaden, 2022).
- [17] C. M. Bender and S. A. Orszag, *Advanced Mathematical Methods for Scientists and Engineers I* (Springer New York, 1999).
- [18] R. Eichhorn, P. Reimann, and P. Hänggi, *Phys. Rev. E* **66**, 066132 (2002).
- [19] R. Eichhorn, P. Reimann, and P. Hänggi, *Phys. Rev. Lett.* **88**, 190601 (2002).
- [20] C. Reichhardt and C. J. O. Reichhardt, *Phys. Rev. E* **100**, 012604 (2019).
- [21] Q. Yang, H. Zhu, P. Liu, R. Liu, Q. Shi, K. Chen, N. Zheng, F. Ye, and M. Yang, *Phys. Rev. Lett.* **126**, 198001 (2021).